In-Situ X-ray Diffraction Study of the Crystallization Kinetics of Mesoporous Titania Films

Bradley L. Kirsch, Erik K. Richman, Andrew E. Riley, and Sarah H. Tolbert*

Department of Chemistry & Biochemistry, University of California, Los Angeles, Los Angeles, California 90095-1569

Received: August 15, 2003; In Final Form: June 15, 2004

In this work, we examine the kinetics of titania crystallization in periodic templated mesoporous thin films with a goal of understanding the relationship between atomic-scale crystallization and nanometer-scale structural change. The anatase crystallization proceeds via a surface-nucleation mechanism that rapidly produces relatively large titania grains. The activation energy for this process is about 210 ± 40 kJ/mol. As the crystallization proceeds, the periodic mesoscale order changes as the particles begin to impinge on the pore volume. The activation energy for this nanoscale restructuring is approximately 140 ± 30 kJ/mol, on the same order of magnitude as that observed for the crystallization. By studying the competition between these two processes, we are able to define the optimal conditions for kinetically controlled crystallization of the mesoporous material without appreciable change in the nanometer-scale structure. The grain growth behavior in the wall structure is also examined and is found to be directly affected by the presence of the inherent pore volume. These data contribute to the current understanding of the crystallization process in mesoporous oxide films and may be generally useful for developing crystalline titania-based materials with tunable nanoscale architectures.

Introduction

A great deal of research has been devoted to mesoscale composite materials since the advent of mesoporous silica.[1,2] It has been shown that these materials can exist in lamellar, hexagonal, or cubic polymorphs depending on the concentration and nature of the structure-directing organic phase.[1−3] This tunability has led to a broad range of work aimed at producing a variety of non-silicon-based metal oxides, including alumina, titania, zirconia, niobium oxide, manganese oxide, and tin oxide materials.[4−15] In fact, the general technique has even been extended to many non-oxide-based systems.[16−20] In addition to bulk powders, self-organized materials can also be produced as thin films.[21−30] Such materials are very similar to their bulk counterparts and are produced through surface-nucleation, drop-casting, spin-coating, or dip-coating techniques.[31]

While many of these materials are limited to amorphous metal oxide wall structures, some thin film and bulk mesoporous systems possess the potential for crystalline grains in the inorganic phase while retaining mesoscale order.[8,9,32−40] In particular, mesoporous titania systems can be heated to produce interconnected anatase domains in the periodic wall structure.[8,9,30,40−44] In bulk titania systems, amorphous grains can crystallize into anatase, rutile, or a mixture of these two phases depending on the preparation and initial particle size.[45] For this templated system, however, the phase stability of the grains in the films follows the behavior of small titania nanoparticles;[46,47] initially the wall structure is completely amorphous, but it transforms cleanly to the metastable anatase phase after heating at about 400 °C. Further heating of nanoscale titania at about 900−1000 °C leads to formation of the rutile structure as the titania grains coarsen and fuse to form larger particles. Unfortunately, the heating process can produce particles that are larger than the initial wall dimensions, leading to the loss of mesoscale order during the process of crystallization.[8,9,30,41,42]

Controlling the crystallization of titania in mesoporous films is potentially useful for a variety of applications involving photovoltaics and photocatalysis.[48−53] In photovoltaics, device performance is ultimately a function of electron and hole mobility, and the degree of crystallization of the titania domains is an important variable that contributes to both the band gap of the material and the electron mobility. In photocatalysis, the presence of crystalline anatase material is crucial for the efficacy of some desirable reactions.[53,54] By understanding the crystallization process in the wall structure, one can begin to tune the extent of crystallization and thus the efficiency of a device toward a given process.

In this work, we seek a better understanding of the crystallization process in the wall structure of mesoporous titania films. A modified version of an established literature synthesis is used to prepare cubic titania films, and in-situ X-ray diffraction is used to track the phase stability in both the titania wall and at the nanometer-scale during heat treatment. Using these data, we explore the kinetics of titania crystallization using the Avrami equation to model the crystallization mechanism and the Arrhenius equation to determine an activation energy for this process. We also explore the kinetics of restructuring on the mesoscale and track the growth of anatase crystallites in the framework. By combining all of this information, we learn about the optimal conditions for controlling the interplay between titania crystallization and loss of the *Im*3*m* mesoporous film structure.

Experimental Section

*Im*3*m* cubic mesoporous titania films were synthesized using a procedure adapted from that of Alberius et al.[30] Briefly, titanium ethoxide was hydrolyzed in highly acidic ethanolic solutions containing the triblock copolymer Pluronic P123. After the solution was allowed to age with vigorous stirring for 15

* To whom correspondence should be addressed. E-mail: tolbert@chem.ucla.edu.

10.1021/jp036442p CCC: $27.50
Published on Web 07/29/2004

min, films were prepared on 12 μm thick silicon substrates through evaporation-induced self-assembly using the dip-coating technique.[31] The pulling rate was approximately 1 mm/s. Films were then aged for 4 days at 10 °C in a sealed environment containing an open vessel of water to maintain high humidity.[28] The films were subsequently heat-treated in air at 60 °C overnight, followed by heat-treatment in air at ~170 °C overnight.[30,41] Preliminary studies without these heat treatments yielded films that did not retain order after prolonged exposure to ambient conditions. The film thicknesses were measured to be ~280 ± 20 nm using atomic force microscopy.

In-situ X-ray diffraction (XRD) data were collected on Beamline 6-2 at the Stanford Synchrotron Radiation Laboratory. Low-angle and high-angle data were collected in transmission geometry with the film perpendicular to the beam using 1.38 and 0.88 Å X-rays, respectively. Samples were ramped up to isothermal holding temperatures of 400, 425, and 450 °C over 20 min and held at temperature in air using two Thermcraft, Inc. model RH201-S-APM resistive-heating furnace hemicylinders connected to produce a furnace with a 0.75 in. bore diameter. The furnace was modified with beryllium oxide and mica windows for high-angle and low-angle diffraction experiments, respectively. The data were collected using a Roper Scientific X-ray CCD detector using 60−90 s exposure times.

TEM images were collected using a JEOL 2000FX instrument operated at 200 kV. The nanoscale structure of the titania films was assigned to the *Im*3*m* cubic phase using the XRD data and TEM images, in agreement with previous work.[42,43,55] JCPDS card number 21-1272 was used to identify the crystalline anatase phase.

Results

Typical TEM images of the titania films examined in this study are shown in Figure 1. Images a, b, and c show the as-synthesized material in planes approximately perpendicular to the [111], [110], and [100] planes, respectively. These images demonstrate the initial *Im*3*m* cubic structure of the films prior to heating at the calcination temperatures. The initial lattice parameter for the cubic unit cell was calculated to be 14 nm prior to the thermal treatments. Images d and e show the same material after calcination at 425 °C for 7 and 18 min, respectively. In image d, it is clear that nanoscale anatase titania crystallites have formed in the walls (regions of high contrast), and yet a large degree of periodicity remains in the pores (regions of low contrast). It is also clear that the size of some of the crystallites can be slightly larger than the initial thickness of the titania walls. The same material heated for a longer period of time (image e) clearly shows the loss of this periodicity in the pore structure, along with more crystallites, showing that the crystallization process leads to the deterioration of the mesoscale order. Image f is a typical selected-area electron diffraction pattern taken from a portion of image e. These data, along with high-angle XRD, allow the crystalline titania to be indexed to the anatase phase, with no signal from either brookite or rutile phases observed in the conditions employed in this study.

Figure 2 shows typical low-angle in-situ XRD data collected during isothermal heat treatment of the cubic titania films at 400 °C. Given the *d* spacing and relative intensity of the peak, along with conventional out-of-plane diffraction data and the expected uniaxial contraction of the film, this peak is indexed as the (002) peak[56] following the work of Crepaldi et al.[42] and Grosso et al.[43] Because of constraints on the diffraction geometry in our setup, the more intense (−110) peak could not be clearly separated from the beam stop. Because the data are collected in transmission geometry, this assignment corresponds to planes that are normal to the substrate. This peak is evident at the beginning of the heating, and its intensity initially increases with time due to the changes in X-ray contrast as the triblock copolymer decomposes at high temperature. The diffraction intensity then gradually decreases with time. This calcination behavior is expected as the titania walls begin to condense and crystallize, leading to changes in the mesoscale order in the film.

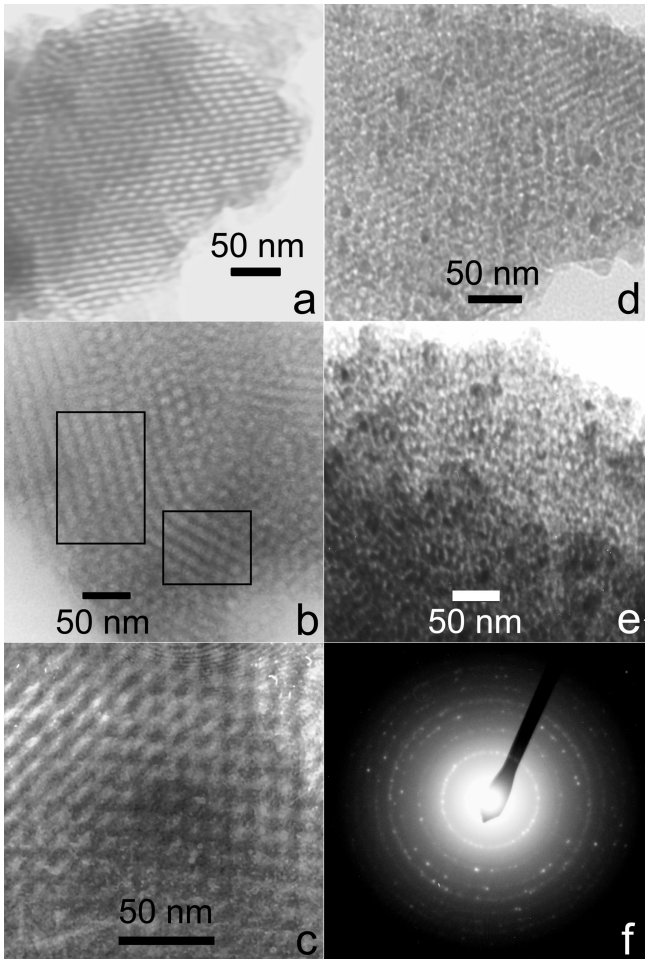

Figure 1. TEM images of as-synthesized (a−c) and calcined (d,e) cubic titania films. The as-synthesized images show planes approximately normal to the (a) [111], (b) [110] (portions highlighted with boxes), and (c) [100] planes. Image d shows a film calcined at 425 °C for 7 min, while image e shows a separate film calcined at 425 °C for 18 min. The pore order is clearly lost after longer calcination times. Image f is an electron diffraction pattern indicative of anatase titania crystallites taken from the material in e.

To examine the low-angle peak behavior as a function of temperature, the XRD data were fit using Gaussians to determine the (002) peak area as a function of time at each of the three isothermal hold temperatures. Figures 3−5 show the results of this analysis for data collected at 400, 425, and 450 °C, respectively (□). All of the films show the same qualitative features observed in Figure 2, with an initial intensity increase to a local maximum followed by a monotonic decrease with time. However, the rates at which these processes occur vary with the treatment temperature. At 400 °C (Figure 3), the area of the peak reaches a maximum value after about 12.5 min at temperature, and significant diffraction intensity persists after 5 h of treatment. In the case of the 425 °C holds (Figure 4), this maximum occurs after about 6.3 min at temperature, and

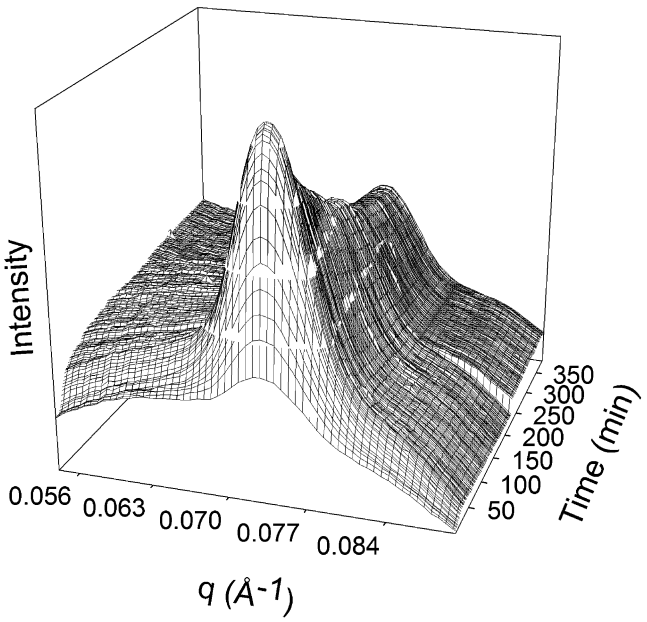

Figure 2. The evolution of the (002) low-angle X-ray diffraction peak collected from an *Im*3*m* cubic mesoporous titania film held at 400 °C. The intensity initially increases due to the decomposition of the triblock copolymer templating species and the accompanying increase in electron density contrast. At all times after the initial maximum, the intensity decreases monotonically.

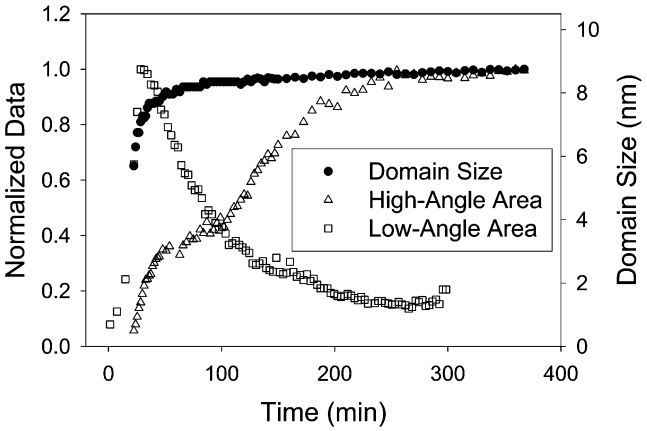

Figure 3. Normalized plots of the low-angle XRD peak area, the high-angle XRD peak area, and the domain size calculated using the Scherrer equation applied to the high-angle XRD. Data were collected during an isothermal hold at 400 °C. At this temperature, the loss of nanometer-scale order approximately anticorrelates with the appearance of atomic scale crystallinity.

the peak area decreases more rapidly than the 400 °C case. Despite this accelerated loss of area, a measurable peak remains beyond 6 h of treatment. At 450 °C (Figure 5), the maximum area occurs after only 4 min at 450 °C, and rapid intensity loss causes the peak to virtually disappear after about 80 min of treatment. These qualitative trends will be discussed further below.

Typical high-angle in-situ XRD data collected on the titania films are shown in Figure 6. Initially, there are no peaks present in the spectra as the wall structure is amorphous on the atomic scale. Holding the material at elevated temperature causes crystallization into the anatase structure, which results in the appearance of the (101) anatase peak. The intensity of this peak increases with further treatment time.

The high-angle XRD data were also fit with Gaussians to measure the area of the (101) anatase peak as a function of

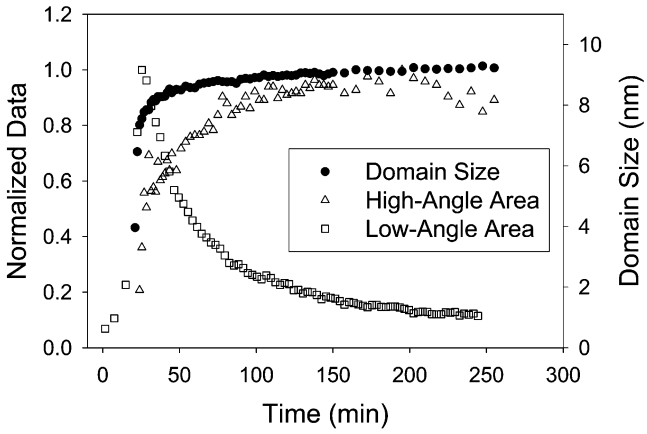

Figure 4. Normalized plots of the XRD peak areas and the domain size collected during an isothermal hold at 425 °C. For this temperature, the appearance of significant crystallinity appears to be faster than the loss of nanometer-scale periodicity.

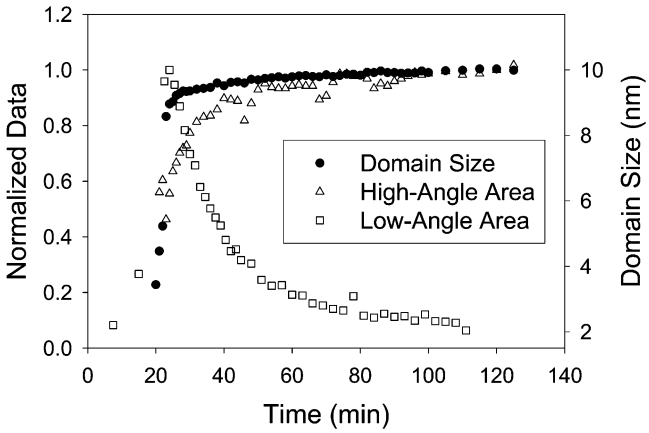

Figure 5. Normalized plots of the XRD peak areas and the domain size collected during an isothermal hold at 450 °C. At this temperature, while all rates are increased, the loss of nanometer-scale periodicity is much slower than the rate of crystallization of the titania walls, resulting in the ability to produce significant crystallization while retaining significant nanometer-scale structure.

time at each of the three isothermal hold temperatures, and the results are shown in Figures 3−5 (△). At 400 °C (Figure 3), the peak begins to appear after about 4.5 min at temperature, and then grows at a moderate rate. At longer times, the area increases at a much slower rate. Heat treatment at 425 °C (Figure 4) puts the onset of crystallization at about 2.5 min, and the (101) peak area initially increases more rapidly than that in the 400 °C data, followed by similar slow growth at later times. Finally, in the case of the 450 °C treatment (Figure 5), the anatase peak begins to appear after holding for approximately 1.3 min. The peak area grows much more rapidly than in the lower temperature data, and the absolute intensity is also much larger.

Examining both the low-angle and the high-angle XRD data together in Figures 3−5 reveals that there is phase coexistence between the *Im*3*m* mesoscale order and the atomic-scale order for at least a short period of time at all of the temperatures studied. With these plots, it is clear that the mesoscale order changes and deteriorates as the wall structure crystallizes. To quantify this deterioration, it is instructive to compare the normalized low-angle peak area remaining after 80% of the normalized high-angle peak area has been achieved. For the 400 °C data (Figure 3), this point occurs after 170 min with about 24% of the nanoscale order remaining. At 425 °C (Figure 4), this point is observed after 70 min with approximately 38%

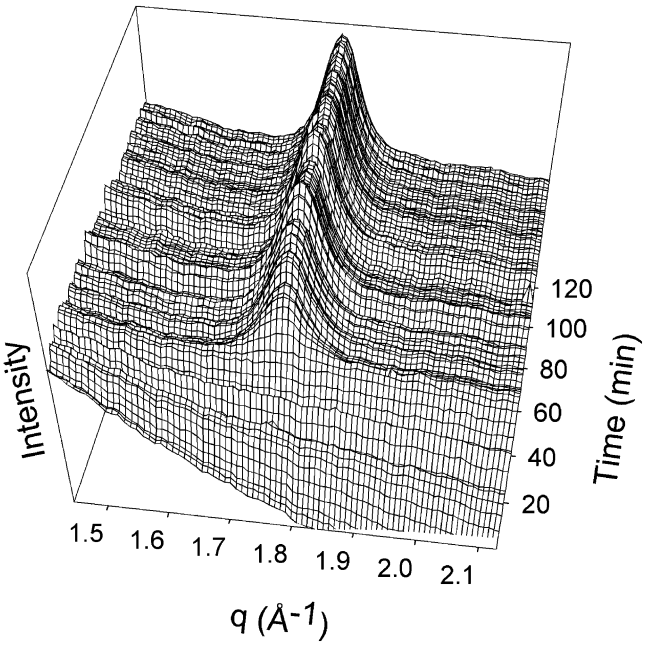

Figure 6. The evolution of the (101) anatase high-angle X-ray diffraction peak collected from a cubic mesoporous titania film at 450 °C. The material begins in the amorphous state and starts crystallizing into the anatase phase after approximately 1 min at 450 °C. The intensity increases quickly at shorter times and then reaches a limiting value at longer times.

of the mesoscale (002) peak area remaining. The data collected at 450 °C (Figure 5) show that this point is achieved after only 30 min with about 66% of the low-angle peak area left. From these data, one observes that at higher temperatures, more of the low-angle order is retained after crystallizing relatively large amounts of the wall structure.

It is also interesting to consider the domain size of the anatase crystallites that form in the titania walls and to track domain size changes with temperature. All of the domain size data in Figures 3−5 (●) are calculated from the full width at half-maximum intensity of the (101) anatase peak.[57] At all of the isothermal hold temperatures, the domain size initially increases very rapidly, followed by a small amount of much slower grain growth over time. For the three experimental hold temperatures, the crystallites reach a domain size that is 90% of their maximum size in only 48, 36, or 26 min for the 400, 425, and 450 °C holds, respectively. While there clearly is some temperature dependence to the 90% domain size times, the times are all much shorter than those needed for the anatase peak area to reach 90% of the maximum area. The results indicate that the crystallization mechanism may not proceed by classic nucleation and growth. In fact, we will argue below that the crystallization is purely nucleation dominated − a phenomenon that has been observed for solid−solid phase transitions in isolated nanocrystal systems.[58,59]

Discussion

From the data presented above, it is clear that the wall structure in mesoporous titania thin films can be crystallized into the anatase structure, and that doing so changes the degree of mesoscale order. It is also clear that the anatase grains grow in a process that is initially very rapid, and then slows down considerably at longer times. To further understand the molecular basis for these changes, kinetic analysis of the activation energies, crystallization mechanism, and grain growth behavior can be carried out using the in-situ XRD data.

A. Crystallization Kinetics and Changes in Nanometer-Scale Structure. Many solid-state phase transitions have been studied using in-situ techniques to follow the amount of material that has reacted. The resulting data are often well described using the integrated form of the Avrami equation

$$-\ln(1-\alpha) = (kt)^n \tag{1}$$

where α is the amount of transformed material, k is the temperature-dependent rate constant, t is time, and n is a parameter that describes how the transformation propagates through the material.[60] In the derivation of eq 1, n contains terms describing both the number of steps involved in nucleation and the number of dimensions in which the nuclei grow.[61] Because there are two processes described, experiments that give identical n parameters can actually refer to different transformation mechanisms, as the n value does not necessarily reflect a unique measurement of both events. In crystallization transformations, nucleation of crystallites may begin in the bulk of the material or at the surface, and as a result the corresponding n parameters vary according to the specific crystallization mechanism. In nucleation-dominated systems that exhibit surface-nucleated crystallization, the n parameter usually has a value of 1.[62] Bulk-nucleated crystallization processes generally produce n parameters that are larger than 1 and include both the nucleation and the growth steps of the transformation.[63]

To analyze isothermal data, the Avrami equation can be rearranged to find the value of the n parameter using

$$\ln(-\ln(1-\alpha)) = n \ln t + c \tag{2}$$

where c is a constant that contains the rate constant k. An n parameter can be obtained from the slope of a linear fit to this equation using fractional transformation versus time data. Once this parameter is known, the peak area data can be fit with the Avrami eq 1 to obtain the rate constant k and the corrected time, which is the difference between the beginning of the isothermal hold and the onset of the crystallization. Assuming that the temperature dependence of the rate constant can be described by the Arrhenius equation, then the equation

$$\ln k = \ln A - E_a/(R \cdot T) \tag{3}$$

can be used to plot the rate constants at various treatment temperatures versus $1/T$ to give a value for the activation energy of the transformation. While this analysis has been applied to a variety of solid−solid phase transitions in the literature, there are inherent limitations in this treatment that lead to activation energies that should be considered approximate values.[61]

To begin understanding the titania crystallization transition, it is interesting to consider the Avrami n parameter as it applies to the high-angle XRD data. All of the data collected at each of the treatment temperatures were fit to eq 2, and typical plots and linear fits are shown in Figure 7A. The average n parameter was observed to have a value of 0.9 ± 0.1. This value is very close to $n = 1$ and is thus attributed to surface-nucleation-dominated crystallization processes.[62] In these porous systems, anatase crystallization could preferentially nucleate at the surfaces and then be essentially complete almost instantly due to the high surface-to-volume ratios found in these nanostructured films. An n value of 1 could also be attributed to bulk nucleation followed by one-dimensional propagation of the transformation front,[63] but it seems unlikely that the crystallization would nucleate in the small amount of bulk film and propagate in one dimension through the three-dimensional cubic nanostructure present in the films.

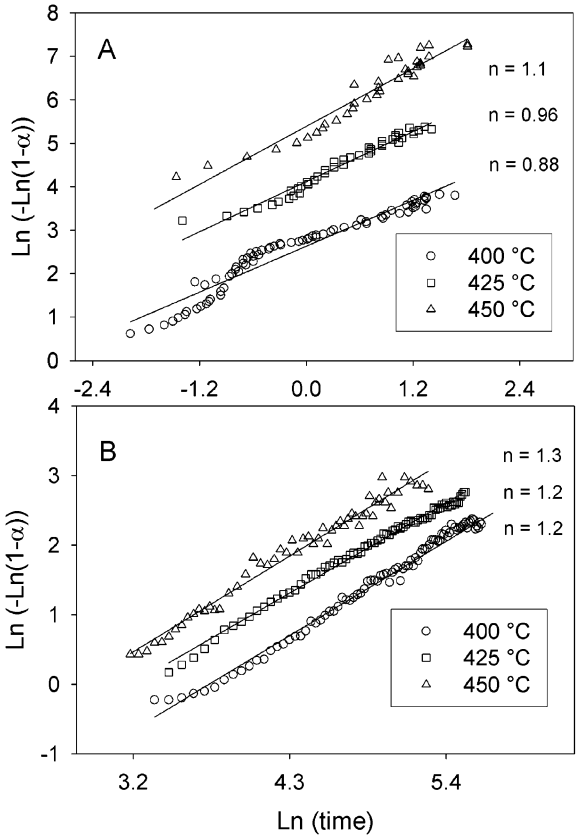

Figure 7. Plots of the modified Avrami eq 2 to determine the value of the *n* parameter for (A) crystallization of anatase titania using high-angle XRD data and (B) loss of nanometer-scale periodicity using low-angle XRD data. The average values of *n* are 0.9 ± 0.1 and 1.3 ± 0.4, respectively. A full discussion of the data is presented in the text.

To further explore the nature of the crystallization, plots of the *n* parameter were examined over different regions of time within individual heating experiments at each of the three treatment temperatures.[64] All of these plots indicated that the *n* parameter varied by a maximum of approximately 0.3 units, indicating that the crystallization mechanism does not vary drastically with time during the isothermal holds. Exarhos et al.[65] have observed similar crystallization behavior in high surface area titania nanoparticle films and found an *n* value around 1.5. Similar results of an *n* parameter near unity have also been found for the crystallization of zirconia nanoparticles.[66]

With the *n* parameter derived from the high-angle XRD data, it is possible to estimate an activation energy for the crystallization of the titania wall structure. The high-angle data were first fit using the Avrami model to calculate the average rate constant at each temperature. The results of this process for representative data collected at 400 °C are shown in Figure 8. The Avrami model describes the data well, and the resulting *k* values from all of the fits were averaged and applied to eq 3.

The corresponding Arrhenius plots and linear fits to derive the activation energy are shown in Figure 9. The slope of the line indicates that the activation energy is about 210 ± 40 kJ/mol. This value is larger than the activation energy of about 142 kJ/mol found for the crystallization of sol−gel-derived nanocrystalline titania thin films.[65] This variation may be due to the different constraints present in the periodic mesoporous film as compared to a film with randomly oriented pores. In the case of the templated mesoporous materials, it may require more energy to create a critical nucleus of crystallized titania in the material due to the constraints of the nanoscale periodicity. In the standard disordered microporous films, these motions may

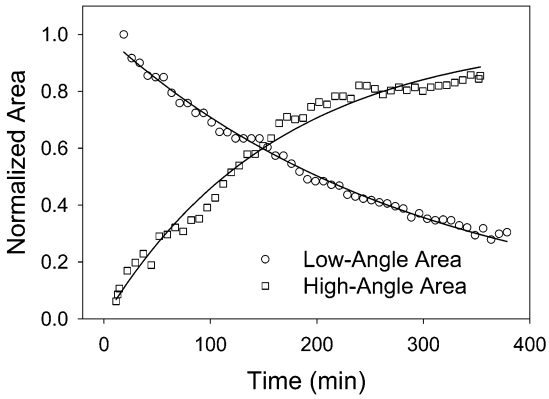

Figure 8. Low-angle and high-angle XRD peak area data fit using the Avrami eq 1 with an *n* parameter of 1 for data collected at 400 °C. The data are well described using this model, and the resulting fits provide the rate constants for restructuring of the nanometer-scale architecture of the films and for crystallization of anatase titania domains, respectively.

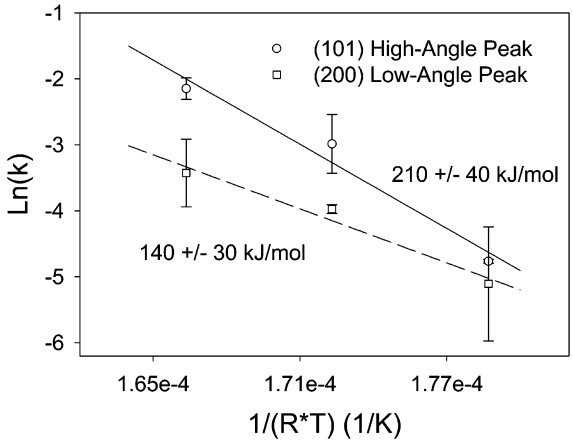

Figure 9. Arrhenius plots showing the temperature dependence of the rate constants for anatase titania crystallization and restructuring of the mesoscale order in templated titania films as measured using XRD data. The slopes of the best fit lines give activation energies of 210 ± 40 kJ/mol for crystallization and 140 ± 30 kJ/mol for changes in nanoscale order. The two lines cross at 380 °C, indicating that at all temperatures above that point, crystallization occurs more rapidly than the loss of the *Im*3*m* nanoscale periodicity.

be relatively energetically favorable because crystallite shape or size changes are less inhibited. The mesoporous material is also very homogeneous in comparison to a random porous film. This homogeneity would not allow relatively low energy nucleation sites to exist in the periodic mesoporous material, whereas the random porous film would have a wider distribution of nucleation sites. Despite these differences, the activation energy for crystallization is within a factor of 2 of values found for the crystallization of nanoscale zirconia[66] and titania systems.[65]

While the kinetics of crystallization have been examined in random nanoscale titania systems prior to this manuscript, the cubic films present a unique opportunity to examine the kinetics of structural change on the mesoscale that accompanies the anatase crystallization. To draw meaningful comparisons, the loss of the (002) low-angle (i.e., mesoscale) XRD peak area was also examined with respect to the Avrami *n* parameter. Typical plots of eq 2 are shown in Figure 7B, and the resulting linear fits produce an average *n* parameter of 1.3 ± 0.4. This value is again close to an *n* parameter of 1. Neither a surface-nucleated transformation nor a one-dimensional transformation front makes significant sense for the degradation of the cubic

nanometer-scale periodicity. As a result, the only way to explain the measured *n* value near 1 is to postulate that the observed changes in the mesoscale (002) planes are intrinsically kinetically linked to the surface-nucleated crystallization process just discussed. This idea agrees well with the observation that mesoscale order is only lost upon the onset of crystallization in mesoporous titania films.[30] Analysis of the *n* parameter on local time scales again showed no significant deviation of the *n* value during the isothermal hold, indicating that the transformation mechanism is constant on the time scale of the experiments.

It is also interesting to compare the activation energy for the change in mesoscale order to the activation energy of anatase crystallization. Figure 8 shows that the Avrami model with an *n* parameter of 1 describes the loss in low-angle peak area very well. Averaged rate constants were again applied to eq 3, and the results of the activation energy analysis for the low-angle XRD data at the three isothermal treatment temperatures are shown in Figure 9. The line of best fit gives an approximate activation energy of 140 ± 30 kJ/mol. If the crystallization and deterioration processes were exactly correlated, one might expect that the two activation energies would be similar. Because they are not equal, it is clear that the correlation is not perfect. However, both XRD and TEM clearly show that the transitions are highly anticorrelated, implying that the processes are, in fact, related. This seems reasonable considering that the estimated activation energy for mesoscale restructuring is less than that of crystallization. Crystallization appears to be a cooperative process involving many atoms moving simultaneously, and so the rate is more strongly temperature dependent. Restructuring of the nanoscale architecture, by contrast, can occur both by uncorrelated surface atom diffusion and when whole domains crystallize. As a result, nanoscale restructuring may be a lower activation energy, less temperature-dependent process.

With these data, it is now possible to consider the optimal conditions for grain growth in the wall structure while retaining the initial *Im*3*m* structure to the maximum degree. If one examines the activation energy plots shown in Figure 9, it is obvious that they must have a point of intersection because they have different slopes. This point would give the temperature at which the crystallization rate constant is equal to the rate constant of mesoscale structural change. Because the *n* parameters for both reactions are approximately the same, equal rate constants imply equal reaction rates. By extrapolating the two lines, one can thus resolve the regimes in which one would expect the rate of the crystallization reaction to be faster than the rate of the mesoscale change, and vice versa. Performing this analysis for the cubic titania films shows that the point of intersection occurs at about 380 °C. Calcination at temperatures above this value should encourage crystallization and minimize the loss of mesoscale order in the (002) dimension, while calcination below this temperature should have a rate of mesoscale structural change greater than that of crystallization. The difference between the two rate constants becomes more pronounced as the temperature increases.

With this information, it becomes clear that higher temperatures are optimal. Because all rates increase with temperature, however, higher temperature calcinations also require faster treatments to minimize the loss of mesoscale structure. This explains why previous ex-situ experiments have shown optimal crystallization at relatively low temperatures. While the majority of temperatures cited in the literature are above this critical temperature of ~380 °C, most studies utilized longer treatment times (on the order of hours) such that temperatures only slightly above the critical temperature were found to be optimal.[8,9,30,41,42] Similar conclusions about optimal crystallization conditions in mesoporous titania films have also been presented by Grosso et al.[43] In their work, films were quickly calcined at high temperature to produce relatively large proportions of the crystalline anatase phase in the walls.

A final point raised by the work of Grosso et al.[43] should also be mentioned in light of the results presented here. In that work, the authors showed that prolonged annealing at moderate temperature (~300 °C) can lead to better retention of nanoscale periodicity upon titania crystallization. In the language of this manuscript, the activation energy for nanoscale rearrangement can be increased by encouraging titania condensation prior to crystallization. This annealing also increases the crystallization temperature, however, suggesting that titania condensation also raises the activation energy for crystallization. In the end, the authors again concluded that the best combination of nanoscale periodicity and atomic scale crystallinity could be achieved by rapid heating at high temperature. Thus, although the detailed activation energies applicable to any given nanoporous titania system are likely to change with the specific chemical and thermal synthesis conditions employed, the general conclusion of high temperature and short time derived from our kinetic data appears to be robust.

B. Grain Growth Kinetics. In conjunction with the activation energies discussed above, it is quite interesting to explore the dynamics of grain growth in the nanostructured films. It is well known that nanoscale crystallites in ceramic systems coarsen to larger average grain sizes upon heat treatment. This process is often a complicated combination of densification, particle fusion, and grain boundary diffusion. The kinetics of grain growth are known to be affected by many different parameters, including the average grain size of the particles prior to sintering, the presence of solute species, and the presence of pores.[67] Because many of these processes are intimately associated with the surface of nanoscale materials, it is interesting to consider the effect of the film geometry on the grain growth behavior by examining the domain size data shown in Figures 3−5.

At all of the isothermal hold temperatures, the domain size initially increases very rapidly, followed by a period of very little grain growth. This supports the observation of an Avrami *n* parameter equal to 1 in the high-angle data discussed above, because $n = 1$ is assigned to a nucleation-dominated process. For data collected at 400 °C (Figure 3), this phenomena is particularly clear as crystallization is slow and the maximum grain sizes are clearly reached long before the maximum extent of crystallization. The same situation exists at the higher treatment temperatures (Figures 4 and 5), but the effect is less pronounced because the kinetic rate constants for crystallization are larger at higher temperatures. The maximum domain sizes observed (ca. 8.5−10 nm) are all in reasonable agreement with the wall thicknesses seen in the TEM experiments (Figure 1).

To model our grain growth data, we attempt to draw on the extensive literature in this area. The kinetics of grain growth in ceramic systems, including nanoscale titania particles,[68] can often be modeled with an empirical rate law of the form

$$D^m - D_o^m = kt \tag{4}$$

where D is the instantaneous grain size, D_o is the initial grain size, and m is the grain growth exponent.[67] Theoretical calculations have shown that the value of m is a function of the grain growth mechanism present in the system. Normal grain growth in a pure, single-phase system should yield $m = 2$, while grain growth in the presence of solutes or pores should give $m = 3$

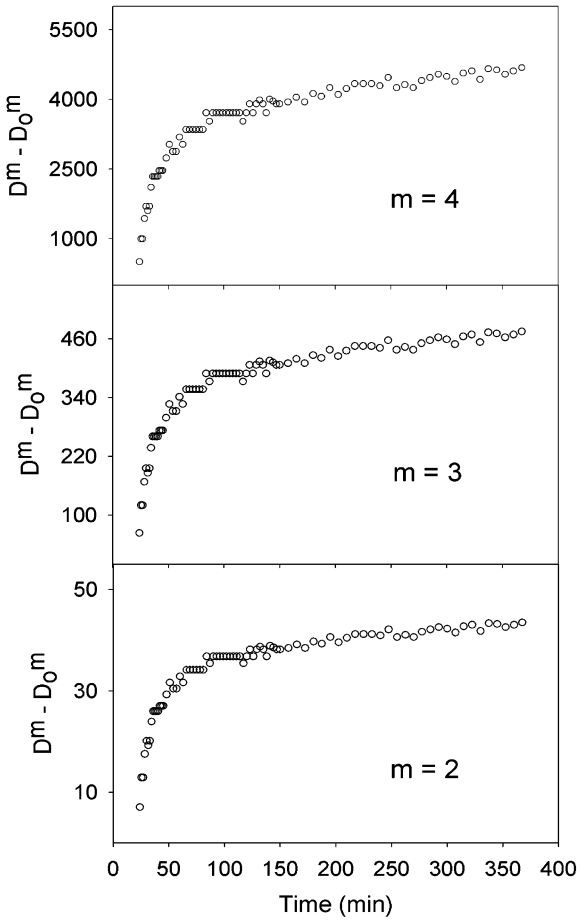

Figure 10. Plots of eq 4 with varying integer estimates of the *m* parameter. None of the resulting plots are linear, indicating that the empirical rate law commonly used in the literature to describe grain growth is not applicable in the periodic, mesoporous titania film system. The grain growth is postulated to proceed via a pure nucleation or "popcorn" mechanism that is discussed in the text.

or $m = 4$.[67,69] To compare our periodic mesoporous materials with disordered nanoscale ceramics, eq 4 was applied to the high-angle XRD data. Using integer estimates for the *m* parameter, one can compare the resulting data to the theoretical linear relationship, which should have a slope equal to the rate constant.[70] While previous authors have successfully applied this technique to micrometer scale particles, less than satisfactory results of the analysis for this kinetic model are shown in Figure 10. Linear fits produced R^2 values near 0.6, indicating that this rate law is not applicable to this templated film system. This may be because the model assumes that growth is dependent on isotropic grain boundary diffusion.[71] This assumption breaks down in the case of our highly ordered cubic titania films because crystallite growth is rapidly attenuated as the size of the domain reaches the dimensions of the titania walls.

The domain size data and the results presented in Figure 10 indicate that the crystallization phenomena seen in this system can be described using a pure nucleation model − something that we sometimes call a "popcorn" model. In popping corn, overcoming the energy barrier for popping leads to rapid production of the popped material, which is relatively homogeneous throughout the volume of the popped kernel. The size of the popped state is generally limited by the initial size of the kernels prior to heating. In the film system, crystallization nucleates at a pore surface and grain growth quickly proceeds through the wall until it encounters another pore. The activation

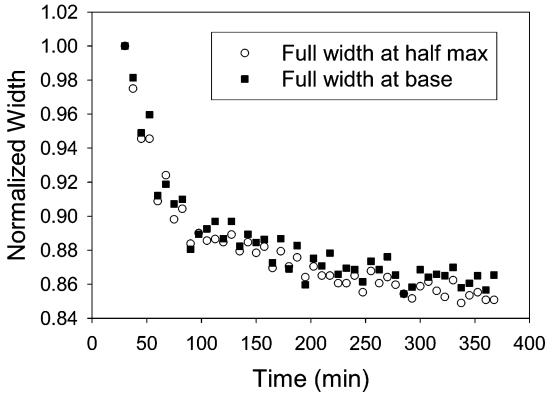

Figure 11. Normalized full width at half-maximum intensity and full width at the base for a Voigt peak applied to the high-angle XRD data obtained during isothermal heat treatment at 400 °C. The Voigt function was chosen so that the two widths could be fit independently. The trends in the data from both widths are virtually identical. This indicates that the shape of the domain size distribution does not change with time, thus excluding a model where the measured half-width is dominated by a few large domains that hide the fact that many small domains are formed and then grow.

barrier for this rapid crystallization is based mostly on nucleation, and it obviously produces crystallites that reach a limiting size in a relatively short time (Figures 3−5). The small amount of growth at longer times can be explained by the hypothesis that crystallites can slowly grow or fuse along the wall or that restructuring at the nanoscale can produce an architecture that allows for slightly larger crystalline domains.[43] The concept of pure nucleation-controlled phase transitions has been previously observed in isolated homogeneous nanocrystals undergoing solid−solid phase transitions,[58,59] so the extension of this idea to a homogeneous nanoscale interconnected framework is quite reasonable.

Given this postulate of nucleation-controlled crystallization, it is instructive to reanalyze the shape of the (101) anatase peak in the high-angle XRD data. The data were refit to track the full width at half-maximum intensity (fwhm) versus the full width at the base of the peak (fwb) using a Voigt peak function with two independent widths to analyze the changes in the crystallite size distributions. It is possible that the nearly invariant domain size observed in Figures 3−5 could be the result of a few large domains that form quickly and then dominate the measured fwhm. These large domains could mask the appearance of smaller domains that nucleate and grow in a fashion more consistent with eq 4. If this were the case, however, one would expect the shape of the peak (i.e., the ratio of fwhm: fwb) to change with time as these small domains grew. The results of this analysis for a sample held at 400 °C are shown in Figure 11. Because the two plots are practically indistinguishable from one another, it is clear that the ratio of the normalized widths stays relatively constant during the entire treatment. This means that the particle size distribution does not change with time and particles almost immediately crystallize into the largest domains that the walls will allow. Changes in the high-angle peak intensity are thus dominated by changes in the number of particles undergoing this crystallization, rather than by changes in domain size. This result, which agrees very well with the observed Avrami *n* parameter of eq 1, strongly supports the hypothesis that the crystallization process is dominated by nucleation effects. The small amount of grain growth that occurs after this process can then proceed by some grain boundary diffusion.[43]

Conclusions

The crystallization kinetics of mesoporous titania thin films have been examined using in-situ isothermal X-ray diffraction. The results show that the crystallization likely proceeds via a surface crystallization mechanism that rapidly produces relatively large anatase grains in the mesoporous wall structure. This crystallization process causes changes in the nanoscale order, as seen in the loss of the low-angle (002) peak area. From a kinetic analysis of the data, the activation energy for anatase crystallization is found to be higher than that for nanoscale restructuring. More importantly, on the basis of activation energies and rate constants, the optimal conditions for production of highly crystalline walls with minimal loss of the *Im*3*m* nanometer-scale order in these titania films, and probably other metal oxides as well, are found to involve short times at high temperatures. Rapid thermal annealing processes, such as those developed for semiconductor processing, should produce conditions in which the rate of crystallization is far greater than the rate of nanoscale-order deterioration. These data lead to a greater understanding of crystallization in periodic, nanoporous titania materials. As the electronic properties of crystalline titania are generally considered to be much superior to the amorphous phase, this work is an important step toward the eventual application of these materials in nanoscale electronics.[52]

Acknowledgment. We thank BASF for the donation of the Pluronic P123 triblock copolymer. This manuscript includes data collected at the Stanford Synchrotron Radiation Laboratory (SSRL), which is operated by the Department of Energy, Office of Basic Energy Sciences. This work was supported by the Office of Naval Research under Grants N00014-99-1-0568 and N00014-04-1-0410, by the Beckman Foundation, and by the National Science Foundation under Grants DMR-9807190 and CMS-0307322. S.H.T. is an Alfred P. Sloan Foundation Research Fellow.

References and Notes

(1) Kresge, C. T.; Leonowitz, M. E.; Roth, W. J.; Vartuli, J. C.; Beck, J. S. *Nature* **1992**, *359*, 710.

(2) Beck, J. S.; Vartuli, J. C.; Roth, W. J.; Leonowicz, M. E.; Kresge, C. T.; Schmitt, K. T.; Chu, C. T.-W.; Olsen, D. H.; Sheppard, E. W.; McCullen, S. B.; Higgins, J. B.; Schlenker, J. L. *J. Am. Chem. Soc.* **1992**, *114*, 10834.

(3) Huo, Q. S.; Margolese, D. I.; Ciesla, U.; Feng, P. Y.; Gier, T. E.; Sieger, P.; Leon, R.; Petroff, P. M.; Schuth, F.; Stucky, G. D. *Nature* **1994**, *368*, 317.

(4) Bagshaw, S. A.; Pinnavaia, T. J. *Angew. Chem., Int. Ed. Engl.* **1996**, *35*, 1102.

(5) Antonelli, D. M.; Ying, J. Y. *Angew. Chem., Int. Ed. Engl.* **1996**, *35*, 426.

(6) Ciesla, U.; Schacht, S.; Stucky, G. D.; Unger, K. K.; Schuth, F. *Angew. Chem., Int. Ed. Engl.* **1996**, *35*, 541.

(7) Tian, Z. R.; Tong, W.; Wang, J.-Y.; Duan, N.-G.; Drishnan, V. K.; Suib, S. L. *Science* **1997**, *276*, 926.

(8) Yang, P.; Zhao, D.; Margolese, D. L.; Chmelka, B. F.; Stucky, G. D. *Nature* **1998**, *396*, 152.

(9) Yang, P.; Zhao, D.; Margolese, D. I.; Chmelka, B. F.; Stucky, G. D. *Chem. Mater.* **1999**, *11*, 2813.

(10) Wong, M. S.; Antonelli, D. M.; Ying, J. Y. *Nanostruct. Mater.* **1997**, *9*, 165.

(11) Wong, M. S.; Ying, J. Y. *Chem. Mater.* **1998**, *10*, 2067.

(12) Sun, T.; Ying, J. Y. *Angew. Chem., Int. Ed.* **1998**, *37*, 664.

(13) Linden, M.; Schunk, S.; Schuth, F. In *Mesoporous Molecular Sieves*; Bonneviot, L., Beland, F., Danumah, C., Giasson, S., Kaliaguine, S., Eds.; Elsevier: Amsterdam, 1998.

(14) Soller-Illia, G. J. de A. A.; Louis, A.; Sanchez, C. *Chem. Mater.* **2002**, *14*, 750.

(15) Pidol, L.; Grosso, D.; Soller-Illia, G. J. de A. A.; Crepaldi, E. L.; Sanchez, C.; Albouy, P. A.; Amenitsch, H.; Euzen, P. J. *J. Mater. Chem.* **2002**, *12*, 557.

(16) MacLachlan, M. J.; Coombs, N.; Ozin, G. A. *Nature* **1999**, *397*, 681.

(17) Trikalitis, P. N.; Rangan, K. K.; Kanatzidis, M. G. *J. Am. Chem. Soc.* **2002**, *124*, 2604.

(18) Rangan, K. K.; Trikalitis, P. N.; Canlas, C.; Bakas, T.; Weliky, D. P.; Kanatzidis, M. G. *Nano Lett.* **2002**, *2*, 513.

(19) Trikalitis, P. N.; Rangan, K. K.; Bakas, T.; Kanatzidis, M. G. *Nature* **2001**, *410*, 671.

(20) Riley, A. E.; Tolbert, S. H. *J. Am. Chem. Soc.* **2003**, *125*, 4551.

(21) Yang, H.; Kuperman, A.; Coombs, N.; Mamiche-Afara, S.; Ozin, G. A. *Nature* **1996**, *379*, 703.

(22) Yang, H.; Coombs, N.; Sokolov, I.; Ozin, G. A. *Nature* **1996**, *381*, 589.

(23) Yang, H.; Coombs, N.; Sokolov, I.; Ozin, G. A. *J. Mater. Chem.* **1997**, *7*, 1285.

(24) Lu, Y. F.; Ganguli, R.; Drewien, C. A.; Anderson, M. T.; Brinker, C. J.; Gong, W. L.; Guo, Y. X.; Soyez, H.; Dunn, B.; Huang, M. H.; Zink, J. I. *Nature* **1997**, *389*, 364.

(25) Zhao, D.; Yang, P.; Melosh, N.; Feng, J.; Chmelka, B. F.; Stucky, G. D. *Adv. Mater.* **1998**, *10*, 1380.

(26) Grosso, D.; Balkenende, A. R.; Albouy, P. A.; Ayral, A.; Amenitsch, H.; Babonneau, F. *Chem. Mater.* **2001**, *13*, 1848.

(27) Crepaldi, E. L.; Soler-Illia, G. J. de A. A.; Grosso, D.; Albouy, P. A.; Sanchez, C. *Chem. Commun.* **2001**, *17*, 1582.

(28) Grosso, D.; Soler-Illia, G. J. de A. A.; Babonneau, F.; Sanchez, C.; Albouy, P. A.; Brunet-Bruneau, A.; Balkenende, A. R. *Adv. Mater.* **2001**, *13*, 1085.

(29) Frindell, K. L.; Bartl, M. H.; Popitsch, A.; Stucky, G. D. *Angew. Chem., Int. Ed.* **2002**, *41*, 960.

(30) Alberius, P. C. A.; Frindell, K. L.; Hayward, R. C.; Kramer, E. J.; Stucky, G. D.; Chmelka, B. F. *Chem. Mater.* **2002**, *14*, 3284.

(31) Brinker, C. J.; Scherer, G. W. *Sol−Gel Science: The Physics and Chemistry of Sol−Gel Processing*; Academic Press: Boston, 1990.

(32) Severin, K. G.; Abdel-Fattah, T. M.; Pinnavaia, T. J. *Chem. Commun.* **1998**, 1471.

(33) Lee, B.; Yamashita, T.; Lu, D.; Kondo, J. N.; Domen, K. *Chem Mater.* **2002**, *14*, 867.

(34) Serre, C.; Hervieu, M.; Magnier, C.; Taulelle, F.; Ferey, G. *Chem. Mater.* **2002**, *14*, 180.

(35) Zhang, Z. R.; Hicks, R. W.; Pauly, T. R.; Pinnavaia, T. J. *J. Am. Chem. Soc.* **2002**, *124*, 1592.

(36) Zhang, Z.; Pinnavaia, T. J. *J. Am. Chem. Soc.* **2002**, *124*, 12294.

(37) Mamak, M.; Metraux, G. S.; Petrov, S.; Coombs, N.; Ozin, G. A.; Green, M. A. *J. Am. Chem. Soc.* **2003**, *125*, 5161.

(38) Miyata, H.; Itoh, M.; Watanabe, M.; Noma, T. *Chem. Mater.* **2003**, *15*, 1334.

(39) Katou, T.; Lee, B.; Lu, D.; Kondo, J. N.; Hara, M.; Domen, K. *Angew. Chem.* **2003**, *42*, 2382.

(40) Grosso, D.; Soler-Illia, G. J. de A. A.; Crepaldi, E. L.; Charleux, B.; Sanchez, C. *Adv. Funct. Mater.* **2003**, *13*, 37.

(41) Crepaldi, E. L.; Soler-Illia, G. J. de A. A.; Grosso, D.; Sanchez, C. *New J. Chem.* **2003**, *27*, 9.

(42) Crepaldi, E. L.; Soler-Illia, G. J. de A. A.; Grosso, D.; Cagnol, F.; Ribot, F.; Sanchez, C. *J. Am. Chem. Soc.* **2003**, *125*, 9770.

(43) Grosso, D.; Soler-Illia, G. J. de A. A.; Crepaldi, E. L.; Cagnol, F.; Sinturel, C.; Bourgeois, A.; Brunet-Bruneau, A.; Amenitsch, H.; Albouy, P. A.; Sanchez, C. *Chem. Mater.* **2003**, *15*, 4562.

(44) Takahashi, R.; Takenaka, S.; Sato, S.; Sodesawa, T.; Ogura, K.; Nakanishi, K. *J. Chem. Soc., Faraday Trans* **1998**, *94*, 3161.

(45) Kumar, P. M.; Badrinarayanan, S.; Sastry, M. *Thin Solid Films* **2000**, *358*, 122.

(46) Song, K. C.; Pratsinis, S. E. *J. Mater. Res.* **2000**, *15*, 2322.

(47) Gaynor, A. G.; Gonzalez, R. J.; Davis, R. M.; Zallen, R. *J. Mater. Res.* **1997**, *12*, 1755.

(48) Bach, U.; Lupo, D.; Comte, P.; Moser, J. E.; Weissortel, F.; Salbeck, J.; Spreitzer, H.; Gratzel, M. *Nature* **1998**, *395*, 583.

(49) Kruger, J.; Plass, R.; Cevey, L.; Piccirelli, M.; Gratzel, M. *Appl. Phys. Lett.* **2001**, *79*, 2085.

(50) Arango, A. C.; Carter, S. A.; Brock, P. J. *Appl. Phys. Lett.* **1999**, *74*, 1698.

(51) Breeze, A. J.; Schlesinger, Z.; Carter, S. A.; Brock, P. J. *Phys. Rev. B* **2001**, *64*, 5205.

(52) Coakley, K. M.; Liu, Y. X.; McGehee, M. D.; Frindell, K. L.; Stucky, G. D. *Adv. Funct. Mater.* **2003**, *13*, 301.

(53) Fox, M. A.; Dulay, M. T. *Chem. Rev.* **1993**, *93*, 341.

(54) Abrahams, J.; Davidson, R. S.; Morrison, C. L. *J. Photochem.* **1985**, *29*, 353.

(55) Soler-Illia, G. J. A. A.; Crepaldi, E. L.; Grosso, D.; Durand, D.; Sanchez, C. *Chem. Commun.* **2002**, *20*, 2298.

(56) Given the transmission XRD geometry used in this experiment, we are able to observe the degenerate (002) and (00−2) in-plane reflections. Because of contraction of the film normal to the substrate, the nominal

cubic film symmetry is broken, and thus these planes are not degenerate with the (200), (020), (−200), and (0−20) family of out-of-plane reflections.

(57) Guinier, A. *X-ray Diffraction in Crystals, Imperfect Crystals, and Amorphous Bodies*; Dover: New York, 1994.

(58) Chen, C.-C.; Herhold, A. B.; Johnson, C. S.; Alivisatos, A. P. *Science* **1997**, *276*, 398.

(59) Jacobs, K.; Zaziski, D.; Scher, E. C.; Herhold, A. B.; Alivisatos, A. P. *Science* **2001**, *293*, 1803.

(60) Avrami, M. *J. Chem. Phys.* **1939**, *7*, 1102; **1940**, *8*, 212; **1941**, *9*, 177.

(61) Bamford, C. H., Tipper, C. P. H., Eds. *Reactions in the Solid State; Comprehensive Chemical Kinetics*; Elsevier: New York, 1980; Vol. 22.

(62) Matusita, K.; Sakka, S. *J. Non-Cryst. Solids* **1980**, *38*, 741.

(63) Matusita, K.; Sakka, S. *Bull. Inst. Chem. Res., Kyoto Univ.* **1981**, *59*, 159.

(64) Calka, A.; Radlinski, A. P. *Mater. Sci. Eng.* **1988**, *97*, 241.

(65) Exarhos, G. J.; Aloi, M. *Thin Solid Films* **1990**, *193*, 42.

(66) Kirsch, B. L.; Tolbert, S. H. Unpublished results.

(67) Mayo, M. J. *Int. Mater. Rev.* **1996**, *41*, 85.

(68) Eastman, J. A. *J. Appl. Phys.* **1994**, *75*, 770.

(69) Brook, R. J. *Treatise on Materials Science and Technology*; Academic Press: New York, 1976; Vol. 9.

(70) Alexander, K. B.; Becher, P. F.; Waters, S. B.; Bleier, A. *J. Am. Ceram. Soc.* **1994**, *77*, 939.

(71) Srdic, V. V.; Savic, D. I. *J. Mater. Sci.* **1998**, *33*, 2391.